Journal of Computational Neuroscience 18, 105–121, 2005

A Cellular Mechanism for Graded Persistent Activity in a Model Neuron and Its Implications in Working Memory

JUN-NOSUKE TERAMAE
Brain Science Research Center, Tamagawa University, machida, Tokyo 194 8610, Japan

TOMOKI FUKAI
Brain Science Research Center and Department of Information-Communication Engineering, Tamagawa University, Machida, Tokyo 194 8610, Japan; Laboratory for Neural Circuit Theory, Brain Science Institute, RIKEN, Wako, Saitama 351 0198, Japan

Received May 7, 2004; Revised September 2, 2004; Accepted September 14, 2004

Action Editor: Xiao-Jing Wang

Abstract. Working memory represents the ability of the brain to hold information for relatively short periods of time. Working memory is believed mediated by persistent neuronal firing. A broadly accepted hypothesis is that persistent activity is generated by reverberating synaptic input. However, single cortical neurons capable of showing persistent firing were recently reported. In this modeling study, we propose a cellular mechanism to generate persistent firing of multiple firing rates in single neurons. In the proposed mechanism, bistable concentrations of inositol 1,4,5-trisphosphate (IP_3) and Ca^{2+} is achieved by IP_3 formation and IP_3-induced Ca^{2+} release from stores in multiple subcellular domains. A postsynaptic firing rate-dependent switching of these bistable elements can demonstrate graded persistent firing of the rat entorhinal neurons. Such a firing rate-dependent switching may be extended to a variety of intracellular Ca^{2+} signaling cascades.

Keywords: parametric working memory, calcium store, bifurcation theory

Introduction

Neurons in several brain areas exhibit persistent firing at multiple firing rates. Graded persistent activity has been implicated in parametric working memory (Romo et al., 1999), decision making (Shadlen and Newsome, 2001; Hernández et al., 2002) and oculomotor control (Aksay et al., 2000, 2001), all of which give examples showing that the brain engages analog memory for short periods of time. A widely accepted hypothesis is that persistent firing may be generated by reverberating feedback excitation (Keller and Kamath, 1975; Rosen, 1972; Wang, 1999; Durstewitz et al., 2000; Kitano et al., 2002). Several integrator circuits have been modeled on the basis of this hypothesis (Cannon et al., 1983; Galiana and Outerbridge, 1984; Seung et al., 2000; Koulakov et al., 2002). Recent experimental and theoretical studies, however, have challenged the proposed role of such recurrent circuits.

The intrinsic ability of single pyramidal cells to generate graded persistent activity was demonstrated recently in a slice preparation of rat entorhinal cortex (EC) (Egorov et al., 2002). With blockade of synaptic transmissions in this preparation, activation of muscarinic receptors enabled EC layer V cells to exhibit sustained activity approximately in the theta frequency range, within which the stable firing rate could be changed by an external input. Since muscarine is known to enhance the working memory performance

of animals (Delmas et al., 2004), the intrinsic firing behavior such as revealed in EC layer V neurons may constitute an elementary form of mnemonic process in the brain.

It remains, however, unclear how graded persistent firing can be generated in single pyramidal cells. It is unclear how multiple firing rates can be robustly maintained against noise. Moreover, it is unclear whether such a persistent activity may subserve working memory, since it could be elicited from EC cells only by an unnaturally long stimulus. Here, we propose that the inositol 1,4,5-trisphosphate (IP_3)-induced Ca^{2+}release (IICR) from stores can underlie graded persistent activity and input integration of single cortical neurons. Muscarinic receptor activation is known to trigger an intracellular signaling cascade leading to IP_3 production (Berridge, 1993; Furuichi and Mikoshiba, 1995), which in turn stimulates specialized Ca^{2+} release sites (Sharp et al., 1993) of the endoplasmic reticulum (ER). We demonstrate in our model that multiple, subcellular compartments that contain Ca^{2+} release sites coupled locally to this signaling cascade can form an ensemble of dynamically bi-stable elements. Stable firing rates can be robustly obtained by activation of different fractions of the bi-stable elements. We show that our model can account for most of the features characteristic of graded persistent firing of the EC cells, providing several experimentally testable predictions regarding the graded firing behavior. In addition, we clarify how we can shorten the critical input duration in this model. Ca^{2+} release from the stores is known to play active roles in neuronal Ca^{2+} signaling in many cells (Furuichi and Mikoshiba, 1995; Berridge, 1998), and this study represents a realistic model to propose a crucial role of Ca^{2+} release in analog memory storage and in computations by single cells.

Methods

Coupled Dynamics of Ca^{2+} Release and IP_3 Production. In our model, IICR plays a central role in maintaining high cytoplasmic $[Ca^{2+}]$ during sustained spike firing. In fact, a muscarine-dependent plateau potential accompanied by spiking was shown to be crucial for persistent firing of EC cells (Egorov et al., 2002). This plateau potential is partially or completely abolished by removal of extracellular Ca^{2+}, intracellular injection of a Ca^{2+} chelator, and by blockade of either L-type Ca^{2+} channels or a Ca^{2+}-activated nonspecific cation current. All these results indicate that graded persistent firing requires a sufficiently high cytoplasmic $[Ca^{2+}]$.

In the cell body and the dendrites of neurons, the ER forms a continuous network that has multiple Ca^{2+} release sites (Berridge, 1998). We assume that the individual release sites are coupled to spatially localized release activators, i.e., voltage-dependent Ca^{2+} channels and an enzymatic reaction cascade leading to IP_3 synthesis. To describe the dynamics of the local $[Ca^{2+}]$, we decompose our model neuron into N (=10) local compartments. In each compartment, the localdynamics of Ca^{2+} are described as

$$\frac{d[Ca^{2+}]}{dt} = J_{Ca} + J_{store,IP_3} + J_{store,leak} - J_{pump,ER} - J_{pump,mem} - J_{exchanger} + J_{diff,Ca}. \quad (1)$$

Each term in the right-hand side is defined as follows. J_{Ca} represents a spike-induced calcium influx into each compartment of the cell through voltage-activated calcium channels. The Ca^{2+} entry is represented as a delta function-like $[Ca^{2+}]$ increase time-locked to every spiking event: $J_{Ca} = j_{Ca}\delta(t - t_{spike})$, where t_{spike} is the time of spike generation and j_{Ca} is the peak amplitude of the influx. As shown in Fig. 5(H) (*right*), the values of j_{Ca} in different compartments are distributed uniformly in a range of 0.013 (the lower bound for triggering Ca^{2+} release) to 0.02 μM.

J_{store,IP_3} and $J_{store,leak}$ represent the rate of IP_3-induced Ca^{2+} release and that of Ca^{2+} leak from the stores, respectively. They are described as

$$J_{store,IP_3} = \mu_{store} P_{open}([Ca^{2+}]_{ER} - [Ca^{2+}]); \quad P_{open} = m_\infty([Ca^{2+}], [IP_3])^3 h^3, \quad (2)$$

and $J_{store,leak} = \mu_{leak}([Ca^{2+}]_{ER}-[Ca^{2+}])$, where $[Ca^{2+}]_{ER}$ is the calcium concentration inside the stores. While the concentration of free Ca^{2+} in the ER is not known, total calcium is in the range of 4–10 mM (Baumann et al., 1991). Since $[Ca^{2+}]_{ER}$ is much higher than the cytoplasmic $[Ca^{2+}]$, $[Ca^{2+}]_{ER}$ is regarded as constant and is set to 1 mM (Fiala et al., 1996) in most of our analyses, except in those devoted for the store refilling mechanism. The open probability P_{open} of the IP_3R depends on activation (m_∞) and inactivation (h) variables. Owing to the inactivation caused by Ca^{2+} binding to the receptors, P_{open} exhibits a bell-shaped dependence on $[Ca^{2+}]$ for a given $[IP_3]$ (De Young and Keizer, 1992). Here, the gating kinetics of IP_3 receptors are described by a model proposed by

Li and Rinzel (1994), which is a neatly reformulated version of the De Young-Keizer model. Thus, the fast activation is represented by the equilibrium value as $m_\infty = [IP_3][Ca^{2+}]/\{([IP_3] + D_{IP_3})([Ca^{2+}] + D_{ACT})\}$, while the slow inactivation variable h satisfies the following equation:

$$\frac{dh}{dt} = a_h \cdot ([Ca^{2+}] + Q)\left(\frac{Q}{[Ca^{2+}] + Q} - h\right), \quad (3)$$

where $Q = D_{INH}([IP_3] + D_{IP_3})/([IP_3] + D_3)$. The following values of parameters are taken from those of the original Li-Rinzel model: $D_{IP_3} = 0.13\ \mu M$; $D_{ACT} = 0.082\ \mu M$; $D_{INH} = 1.05\ \mu M$; $D_3 = 0.94\ \mu M$. The rate constant a_h is set as $10\ \mu M^{-1}s^{-1}$ to avoid intensive Ca^{2+} oscillations. The remaining constants are set as $\mu_{store} = 6.6\times10^{-3}\ s^{-1}$ and $\mu_{leak} = 0.12\times10^{-3}\ s^{-1}$ to produce the experimentally observed time course of Ca^{2+} release (Nakamura et al., 1999, 2000). With these rate constants, the average cytoplasmic $[Ca^{2+}]$ is kept in a range of 0.4–0.5 μM during persistent firing of the model neuron.

Outward fluxes, $J_{pump,ER}$, $J_{pump,mem}$ and $J_{exchanger}$, represent the rates of Ca^{2+} extrusion through the ER and the cell membranes by the ATPase Ca^{2+} pump, and the effulux extruded by the Na^+/Ca^{2+} exchanger through the cell membrane, respectively. They are described as,

$$\begin{aligned} J_{pump,A} &= \mu_{pump,A}\frac{[Ca^{2+}]^2}{[Ca^{2+}]^2 + K_{pump}^2}(A = ER, mem); \\ J_{exchanger} &= \mu_{exchanger}\frac{[Ca^{2+}]}{[Ca^{2+}] + K_{exchanger}}, \end{aligned} \quad (4)$$

by Michaelis-Menten type equations with $K_{pump} = 0.2\ \mu M$ and $K_{exchanger} = 2\ \mu M$ (Yamada et al., 1998). The rate parameters are set as $\mu_{pump,ER} = 0.8\ \mu M^{-1}s^{-1}$, $\mu_{pump,ER} = 0.1\ \mu M^{-1}s^{-1}$ and $\mu_{exchanger} = 2.7\ \mu M^{-1}s^{-1}$ to produce the time course of Ca^{2+} release consistent with experiments.

In many neurons, IP_3 is produced from phosphatidylinositol 4,5-biphosphate (PIP_2), and this production is catalyzed by agonist-induced activation of phospholipase C (PLC). Muscarine is known for one of such agonists (Berridge, 1993). PLC activity depends strongly on the cytoplasmic $[Ca^{2+}]$, and it is modeled as

$$PLC([Ca^{2+}]) = \frac{[Ca^{2+}]^4}{[Ca^{2+}]^4 + K_{PLC}^4}, \quad (5)$$

with $K_{PLC} = 0.57\ \mu M$ (Allbritton et al., 1992). Thus, IP_3 production is modeled as (Fiala et al., 1996)

$$\begin{aligned} \frac{d[IP_3]}{dt} &= \alpha \cdot PLC([Ca^{2+}]) \cdot ([IP_3]_{max} - [IP_3]) \\ &\quad -\beta \cdot [IP_3] + J_{diff,IP_3}, \end{aligned} \quad (6)$$

where α and β represent the rates of IP_3 production and decomposition, respectively. The parameter values are set as $\alpha = 40.0\ (s^{-1})$, $\beta = 8.0\ (s^{-1})$ and $[IP_3]_{max} = 5.0\ \mu M$ (Walker et al., 1987; Wang et al., 1995).

$J_{diff,X}$ ($X = Ca^{2+}$ or IP_3) represents the diffusion of Ca^{2+} or IP_3 between neighboring compartments. As our model consists of discrete compartments, we employ the following discrete version of the diffusion term:

$$D_A\frac{\partial^2[A]}{\partial x^2} \to \frac{D_A}{L^2}([A]_{k+1} + [A]_{k-1} - 2[A]_k), \quad (7)$$

where $[A]_k$ denotes the concentration of Ca^{2+} or IP_3 in the k-th compartment. The effective diffusion coefficients of Ca^{2+} and IP_3 are measured as $D_{Ca} = 13$ and $D_{IP_3} = 280\ \mu m^2/s$, respectively (Allbritton et al., 1992). These diffusion coefficients implicitly take the effect of Ca^{2+} buffuring into account, and we do not include explicit Ca^{2+} buffring dynamics in the present model. L is the typical length scale, i.e., the size of one compartment. We see that the effective strength of diffusion decreases in inverse proportion to the square of L. Therefore, we may neglect the contributions of the diffusion terms if the compartment size is much longer than the typical diffusion range of $[Ca^{2+}]$ and $[IP_3]$.

Membrane Potential. Time evolution of the membrane potential is described by an integrate-and-fire neuron model as

$$\tau\frac{dV}{dt} = I_{input} - I_{leak} - I_{CAT}, \quad (8)$$

where I_{input} represents an applied current and $I_{leak} = g_{Leak}(V - E_{Leak})$ is leak current. When V reaches V_{th}, the cell fires and V is reset to V_{reset}. The parameters are set as $g_{leak} = 0.02$, $E_{Leak} = -65$ mV, $V_{th} = -50$ mV, $V_{reset} = -80$ mV and $\tau = 10$ ms. I_{CAT} is a Ca^{2+}-activated cationic current, which is crucial for persistent firing of EC layer V neurons (Egorov et al., 2002). The Ca^{2+}-activated cationic current is modeled as

$$I_{CAT} = g_{CAT}\sum_{k=1}^{N}\frac{[Ca^{2+}]_k}{[Ca^{2+}]_k + K_{CAT}}(V - E_{CAT}), \quad (9)$$

where $[Ca^{2+}]_k$ stands for the calcium concentration in the k-th compartment. $K_{CAT} = 10\ \mu M$ and the reversal

potential $E_{\mathrm{CAT}} = -40$ mV (Kang et al., 1998; Aoyagi et al., 2002). For the present 10-compartment model, $g_{\mathrm{CAT}} = 0.4$.

Refilling the Calcium Store. Recent experimental studies revealed that Ca^{2+} store is rapidly refilled by 'store-operated' channels (SOCs), which is a calcium-dependent calcium channel on the cell membrane (Parekh and Penner, 1997; Putney and Ribeiro, 2000; Blaustein and Golovina, 2001). When the ER is unloaded, SOCs open and Ca^{2+} enter into the sub-SOC-space of cytoplasm from the extracellular fluid. This Ca^{2+} is then rapidly pumped into the adjacent ER. In most of our analyses, we set $[Ca^{2+}]_{\mathrm{ER}}$ constant assuming that $[Ca^{2+}]_{\mathrm{ER}}$ is kept at a sufficiently high concentration during cell firing. In some simulations, however, we include the following dynamics of $[Ca^{2+}]_{\mathrm{ER}}$ and $[Ca^{2+}]_{\mathrm{SOC}}$, the local calcium concentration of the sub-SOC-space, into our model and investigate the crucial role of the SOC-dependent store-refilling process in graded persistent activity:

$$c_1 \frac{d[Ca^{2+}]_{\mathrm{ER}}}{dt} = \left(J_{\mathrm{pump,ER}} - J_{\mathrm{store,IP_3}} - J_{\mathrm{store,leak}}\right) + \left(J'_{\mathrm{pump,ER}} - J'_{\mathrm{store,IP_3}} - J'_{\mathrm{store,leak}}\right), \tag{10}$$

$$c_2 \frac{d[Ca^{2+}]_{\mathrm{SOC}}}{dt} = J_{\mathrm{SOC}} + J'_{\mathrm{store,IP_3}} + J'_{\mathrm{store,leak}} - J'_{\mathrm{pump,ER}}, \tag{11}$$

where the volume ratios of the ER and the sub-SOC-space to each compartment of the cytoplasm are set as $c_1 = 0.1$ and $c_2 = 0.2$, respectively. $J'_{\mathrm{pump,ER}}$, $J'_{\mathrm{store,IP_3}}$ and $J'_{\mathrm{store,leak}}$ are the calcium fluxes between the ER and the sub-SOC-space. Their dynamics obey Eqs. (2), (3) and (4), in which $[Ca^{2+}]$ is replaced with $[Ca^{2+}]_{\mathrm{SOC}}$. The rate constants of these fluxes are set as $\mu'_{\mathrm{store}} = 1.0 \times 10^{-3}\ \mathrm{s}^{-1}$, $\mu'_{\mathrm{leak}} = 1.0 \times 10^{-2}\ \mathrm{s}^{-1}$ and $\mu'_{\mathrm{pump,ER}} = 1.0 \times 10^{-2} \mu\mathrm{M}^{\mathrm{tx}}\mathrm{s}^{-1}$. Since the effective diffusion length of IP_3 is much larger than that of Ca^{2+}, $J_{\mathrm{IP_3}}$ and $J'_{\mathrm{IP_3}}$ are gated by the same $[IP_3]$ obeying Eq. (6). J_{SOC} is a Ca^{2+} influx through SOC. Since the detailed dynamics of the SOC remain unknown, we modeled J_{SOC} as

$$J_{\mathrm{SOC}} = \mu_{\mathrm{SOC}} \frac{K_{\mathrm{SOC}}}{[Ca^{2+}] + K_{\mathrm{SOC}}}. \tag{12}$$

Setting $K_{\mathrm{SOC}} = 1.0\ \mu\mathrm{M}$ and $\mu_{\mathrm{SOC}} = 2.0 \times 10^{-3}\ \mu\mathrm{M}^{-1}\mathrm{s}^{-1}$ maintains the calcium concentrations in the cytoplasm, ER and sub-SOC-space always at proper levels.

All the numerical integrations were programmed by C or C^{++} programming language and run on an Athlon AMD processor.

Results

IP_3 and Calcium Signaling

In our model, nonlinear dynamics of Ca^{2+} and IP_3 are represented by multiple subcellular compartments, each containing a localized Ca^{2+} release site and a phospholipase C (PLC) signaling cascade leading to IP_3 production (Fig. 1). These compartments act as bi-stable elements during neuronal firing, if they are sufficiently separated from each other and the diffusion of Ca^{2+} and IP_3 couples them only moderately. The model is based on the following physiological properties of cortical neurons: (1) The cell body and dendritic shafts of pyramidal neurons show a significant degree of IICR, as was demonstrated in the hippocampal CA1 pyramidal neurons (Nakamura et al., 1999, 2000); (2) In many cells including cortical pyramidal neurons, activation of cholinergic muscarinic receptors activates a G protein, which in turn activates PLC, crucial for IP_3 production (Berridge and Irvine, 1989; Berridge, 1998); (3) An isozyme of PLC, for instance brain-abundant PLC-βs shows Ca^{2+}-dependent activity (Mignery et al., 1992); (4) The IP_3Rs coupled

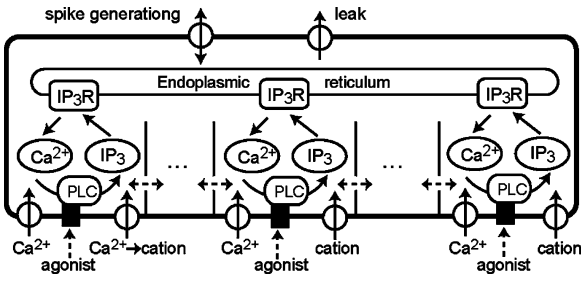

Figure 1. The model neuron consisting of an ER network and multiple Ca^{2+} and IP_3 domains. In this study, the model has 10 subcellular compartments. Spiking elevates $[Ca^{2+}]$ in the individual compartments, with different peak amplitudes in different compartments. Phospholipase C (PLC) is activated by agonist (e.g., acetylcholine) binding to receptors and regulates IP_3 production. In each compartment, binding of Ca^{2+} and IP_3 to IP_3Rs activates the IP_3R-channels to release Ca^{2+} into the cytoplasm. Since the brain-abundant PLC activity has a Ca^{2+}-dependent component, IP_3 and Ca^{2+} can form a positive feedback reaction cycle. This positive feedback loop is crucial for the bistability of each subcellular compartment. In some simulations, diffusion of Ca^{2+} and IP_3 is included between neighboring compartments.

to their activators are considered to be localized in the intracellular space (Berridge, 1993; Sharp et al., 1993; Furuichi and Mikoshiba, 1995); (5) Ca^{2+} influx through voltage-gated Ca^{2+} channels shows large fluctuations along the dendrites (Spruston et al., 1995); (6) As indicated in EC cells (Egorov et al., 2002), Ca^{2+}-activated nonselective cation current translates information stored by the cytoplasmic Ca^{2+} into output firing rate (Kang et al., 1998; Partridge and Valenzuela, 1999).

During spiking, rapid increases of $[Ca^{2+}]$ occur in the individual compartments, promoting Ca^{2+} binding to IP_3Rs. The IP_3R-channel opened by binding of Ca^{2+} and IP_3 releases Ca^{2+} into the cytoplasm to further facilitate the Ca^{2+} release and IP_3 production. The Ca^{2+}-dependence of PLC activity implies two important facts in our model: IP_3 production can be facilitated by the $[Ca^{2+}]$ increase during spiking; IP_3 and Ca^{2+} may form a positive feedback cycle in enzymatic reactions. As demonstrated later, these properties are crucial for the dynamical bistability of the Ca^{2+}-IP_3 compartments. The compartmentalization of the subcellular space is necessary for keeping the multiple Ca^{2+}-IP_3 systems relatively independent. In many cells, products of the PLC signaling can modify the activity of a wide variety of downstream targets (Berridge, 1998). To ensure specificity and speed of signal transduction events, various components of the PLC signaling pathway are restricted in specifically designed subcellular microdomains (Delmas et al., 2004). Hence the compartmentalization in this model is not biologically unrealistic. To be specific, the number of the compartments is fixed at 10, although the performance of this model does not crucially depend on a specific choice of this number. We examine to what extent the diffusion of Ca^{2+} and IP_3 between neighboring compartments influences the graded firing behavior of this model. For the time being, the diffusion effects are not included in order to elucidate the essential mechanism of information coding.

Postsynaptic Firing Rate-Dependent Bi-Stability of the Ca^{2+}-IP_3 Reaction System

We depict how the dynamical bistability is achieved in our model. Figure 2(A) illustrates the bell-shaped profile of Ca^{2+} flux released from Ca^{2+} stores (Bezprozvanny et al., 1991). At low $[Ca^{2+}]$, Ca^{2+} acts as a coagonist with IP_3 and facilitates IICR, whereas at higher

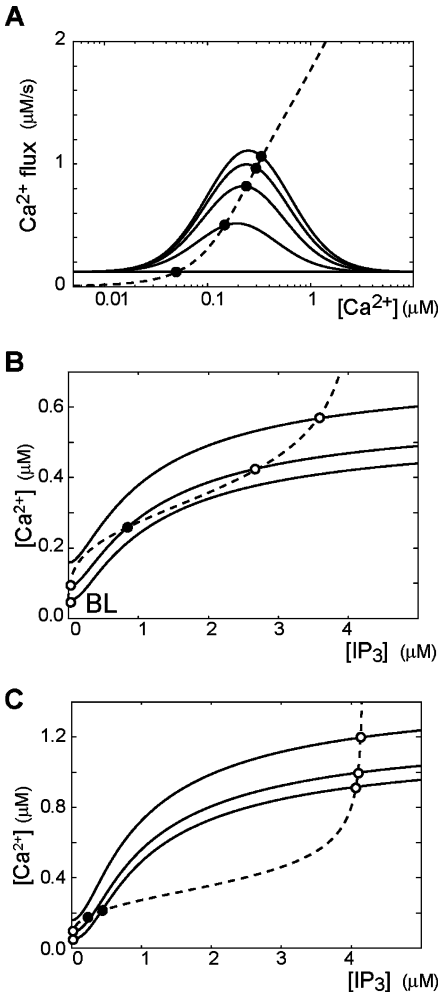

Figure 2. Bi-stable property of local $[Ca^{2+}]$ and $[IP_3]$. (A) The calcium release rate of the IP_3R-channels shows a bell-shaped profile with respect to cytoplasmic $[Ca^{2+}]$ (solid curves). The peak rate increases as $[IP_3]$ increases, as indicated for $[IP_3] = 0$, 0.5, 1, 1.5 and 2 (μM), displayed respectively from bottom to top. Intersection of each bell-shaped curve (black circles) and the curve indicating the Ca^{2+}-pumping rate (dashed curve) gives the stationary Ca^{2+} concentration ($[Ca^{2+}]_0$) for a given $[IP_3]$. (B) The dependence of $[Ca^{2+}]_0$ on $[IP_3]$ is shown for 3 different firing frequencies: 0 (bottom solid), 6 (middle) and 12 Hz (top). Because of the Ca^{2+} influx associated with spiking, $[Ca^{2+}]_0$ rises with an increase in firing rate. The stationary $[IP_3]$ reached by IP_3 production is depicted by a dashed curve. Intersections of this curve with any of the solid curves give the stationary values of the time-averaged $[Ca^{2+}]$ and $[IP_3]$ at the corresponding firing rate (white circles). In this model, bi-stability appears in an intermediate frequency range (middle curve: black circle represents unstable point). BL, baseline. (C) Suppression of the IP_3R-channel inactivation shifts upwards the solid curves representing $[Ca^{2+}]_0$. Consequently, the states of low $[Ca^{2+}]$ may acquire only narrow basins of attraction, if they remain stable.

concentrations, Ca^{2+} inhibits IP_3R opening and blocks Ca^{2+} release. The Ca^{2+} efflux pumped back into the stores and extruded from the cell membrane is represented by the dashed curve. Suppose that the neuron is in the resting state. Then, at a given $[IP_3]$, the steady-state $[Ca^{2+}]$ in a compartment is determined by the balance between the inward flux into and the outward flux from the cytoplasmic space, which is ensured at the intersection of the two curves in Fig. 2(A) (black circles). Here, we simply assume that the Ca^{2+} inside the ER membrane is not exhausted by the release. The refilling process will be considered later. Figure 2(B) illustrates how the intersection of the curves changes with $[IP_3]$ in the $[Ca^{2+}]$-$[IP_3]$ plane (bottom solid curve). Baseline $[Ca^{2+}]$ and $[IP_3]$ (point BL) are determined as the intersection of the blue curve and a dashed curve representing the $[IP_3]$ reached through IP_3 production at any given $[Ca^{2+}]$ (Meyer and Stryer, 1988; Wagner et al., 2004). Now, let the neuron fire at a constant rate. During firing, additional Ca^{2+} influx enters into the neuron, raising the average cytoplasmic $[Ca^{2+}]$ at an arbitrary $[IP_3]$. Such influx causes the blue curve to shift upwards along the $[Ca^{2+}]$ axis such that bi-stable states may appear in an intermediate range of firing frequency (middle solid curve). Due to cell firing, the stationary $[Ca^{2+}]$ cannot be constant, but oscillates with small amplitudes, implying that the bi-stable states are not static. If firing frequency is increased further, the bi-stable state disappears (top solid curve), leaving a monostable state at high $[Ca^{2+}]$ and high $[IP_3]$. Thus, the Ca^{2+}-IP_3 system can be regarded as a bi-stable element acting in a firing rate-dependent way. In this study, parameter values (e.g., the maximal conductance of the Ca^{2+}-activated cation current) are adjusted such that the bistability may appear in a near theta-frequency range.

A characteristic of the IP_3R channel is its bell-shaped profile of the open probability, i.e., the negative feedback effect of Ca^{2+} binding. It seems intriguing to see how the blockade of the IP_3R inactivation affects the bi-stable property. With this blockade, the stationary $[Ca^{2+}]$ achieved by IICR is greatly increased at any $[IP_3]$, as demonstrated by the solid curves in Fig. 2(C). The increased stationary $[Ca^{2+}]$ may create an additional high $[Ca^{2+}]$ state on the bottom curve, while turning the baseline state fragile. Indeed, the baseline state could even disappear if it had a slightly greater $[IP_3]$. Later, we conduct numerical simulations of the neuron model to study the influences of suppressed IP_3R inactivation.

Mechanism of Graded Stable Changes in Ca^{2+} and IP_3 Concentrations

As already demonstrated, the individual Ca^{2+}-IP_3 compartments are bi-stable within certain frequency ranges, and these ranges differ for different compartments owing to the broad distribution of the peak intensity of Ca^{2+} influx. As a result, the model neuron can be regarded as an ensemble of bi-stable elements influenced differentially by a common firing rate. Below, we show how the ensemble of bi-stable elements are activated or deactivated by external inputs to achieve graded rate changes within a limited frequency range.

In the absence of external stimuli, the firing frequency of the model neuron is essentially determined by the average $[Ca^{2+}]$ that acts on Ca^{2+}-activated cation current in each compartment (Kang et al., 1998; Partridge and Valenzuela, 1999). In Fig. 3, the gray curve shows this dependence of firing rate on the average $[Ca^{2+}]$. Each compartment has bi-stable states within a certain frequency range (solid traces). If the model has only a single compartment, two stable states appear: one at low and one at high firing rates (Fig. 3(A)). Likewise, with two compartments, the model can have at maximum three stable firing frequencies (Fig. 3(B)). In this way, the number of stable-firing states increases as the number of compartments increases (Fig. 3(C)).

Figure 3(D) demonstrates how a depolarizing or hyperpolarizing step current determines a new stable firing state in our model. If a depolarizing input is applied to the model neuron, firing rate increases for an arbitrary $[Ca^{2+}]$ (red dashed curve 1-1′). During this input, the stable state of the Ca^{2+}-IP_3 system shifts to a new unique stable state D, given by the intersection of the curve 1-1′ and the solid lines. Thus, the state variables are attracted by this new stable state. If the input is turned off, then the state variables shift back to the gray solid line and settle into a new equilibrium, corresponding to an increased stable firing frequency. By contrast, application of a hyperpolarizing input inhibits firing, as illustrated by the gray dashed curve 2-2′. During this hyperpolarizing input, the state variables are attracted by a unique stable point denoted as H. When the input is terminated, the state variables either arrive at a new equilibrium point, corresponding to a reduced firing frequency, or to point H (the resting state), depending on the state at that moment. As was the case in the electrophysiology experiments, weak

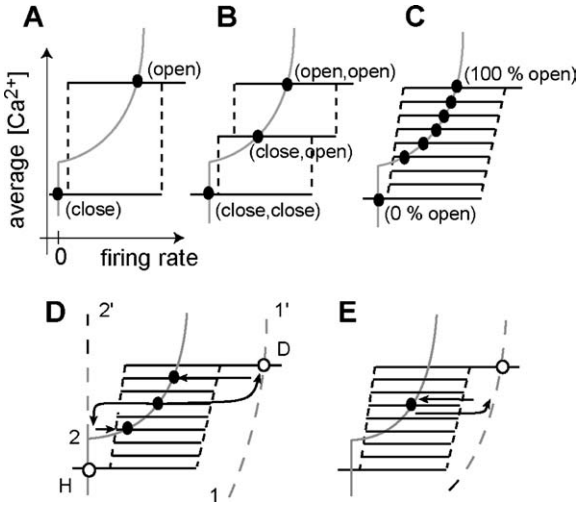

Figure 3. Multiple stable states in an ensemble of bi-stable elements. (A) As shown in Fig. 2(B), a local Ca^{2+}-IP_3 compartment exhibits bi-stability within a certain range of firing rates (solid lines). In the model, information stored by intracellular $[Ca^{2+}]$ is translated into firing rate by a Ca^{2+}-activated cation current (gray curve). Two steady states are indicated at the intersections of these two curves (black circles). (B) A similar diagram is depicted for a model with two local compartments. At maximum, three stable states can appear. (C) Multiple stable states appear in a model neuron with a sufficient number of Ca^{2+}-IP_3 compartments. (D) Effects of an external input on the stable $[Ca^{2+}]$ and $[IP_3]$ in the model. During injection of a strong depolarizing current, the Ca^{2+}-firing rate curve shifts rightwards (1-1′). The state vector is attracted by the unique stable state D. After injection of current, the system settles into a new stable state at a higher $[Ca^{2+}]$. During a hyperpolarizing input, the state vector is attracted by the unique stable state H. After the presentation of input, the state vector settles into either a new stable state at a lower $[Ca^{2+}]$ or the resting state (H). (E) A weak input cannot shift the state vector to a new stable firing state. Thus, the response of the model shows threshold effects.

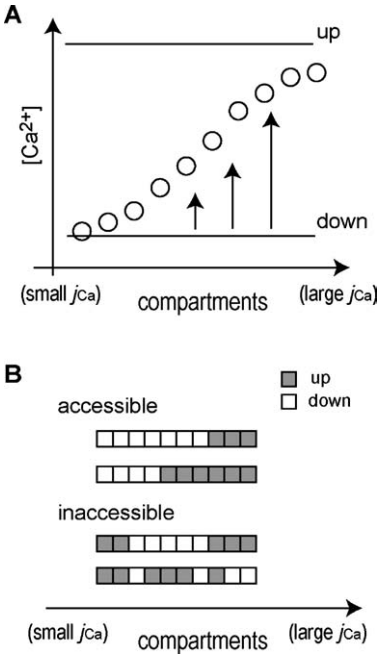

Figure 4. Sequential state transitions in multiple bi-stable elements and the accessible stable states. (A) A larger influx of spike-induced Ca^{2+} entry makes the $[Ca^{2+}]$ in a local compartment more sensitive to spiking firing. Therefore, consecutive inputs always cause the bi-stable transitions of the individual compartments in a fixed ascending or descending order. (B) The upper two states show examples accessible by external inputs, whereas the lower two states cannot be realized by external inputs due to the sequential activation of local Ca^{2+}-IP_3 domains. In this model, the number of accessible states is at most $10 + 1$ (including the resting state).

input in the model cannot induce changes in a stable firing rate (Fig. 3(E)).

In the absence of the diffusion coupling, the model can, in principle, show 2^{10} different stable states since it is composed of 10 independent bi-stable elements. However, the number of the distinct states accessible by an external input is much smaller than 2^{10} and is at most 11 including the resting state, since the bi-stable transitions of the individual compartments can occur only in a fixed ascending or descending order determined by the relative intensity of Ca^{2+} influx. In a compartment with larger j_{Ca}, $[Ca^{2+}]$ is raised more rapidly by an depolarizing input and is decreased more slowly by a hyperpolarizing inputg (Fig. 4(A)). Thus, many states cannot be realized by external stimuli (Fig. 4(B)). In the presence of the diffusion coupling, the number of accessible states may be further reduced since some of them are degenerate.

Graded Persistent Firing of the Model Neuron

To show that graded persistent activity would emerge in the model neuron, we conducted numerical simulations. We found that the firing behavior of the model coincides well with the experimental observations of the EC layer V neurons. A depolarizing step current evoking high-frequency spikes initiated persistent firing in the model neuron, and a second input raised the firing rate to a higher stable rate (Fig. 5(A)). Similarly, consecutive depolarizing inputs raised the firing frequency in a discrete manner until it saturated (Fig. 5(B)). This saturation behavior is a characteristic of the experimentally observed graded persistent activity. Each depolarizing current pulse increased the stationary-state $[Ca^{2+}]$ in some local compartments,

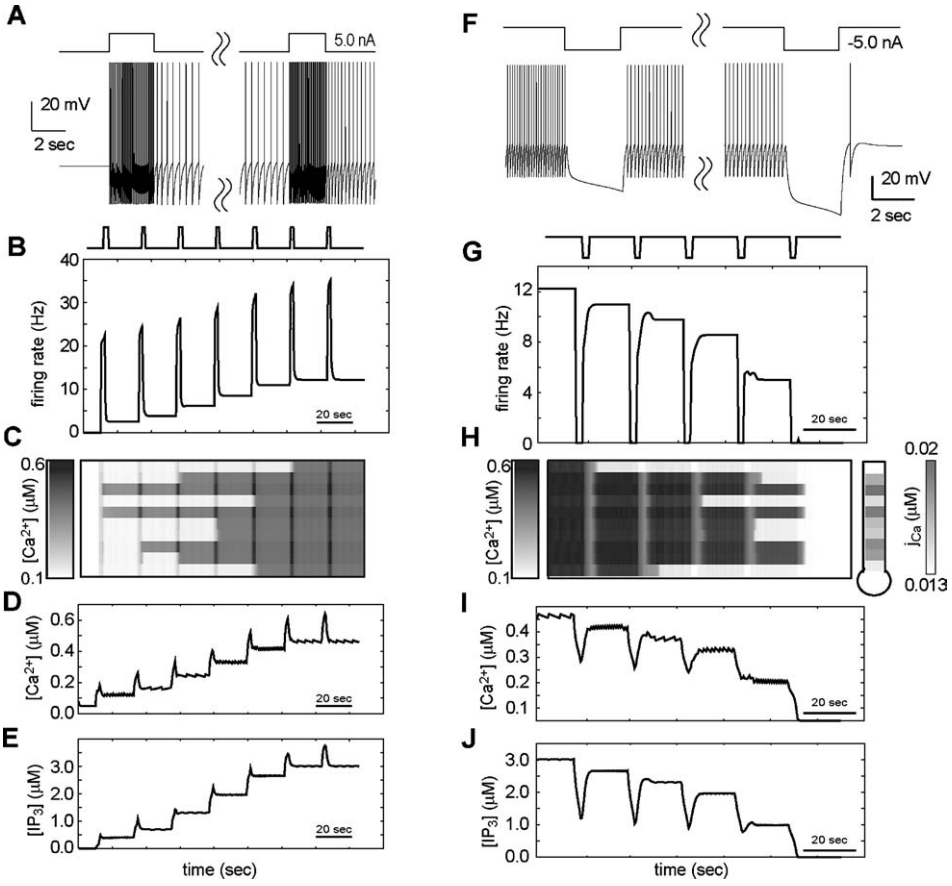

Figure 5. Discrete rate changes induced in the model neuron by consecutive depolarizing or hyperpolarizing step currents. (A) Two depolarizing inputs separated by several seconds are applied to the model neuron. The first input initiates persistent firing and the second one raises the stable-state firing rate. (B) Firing rate of the model neuron increases in a stepwise fashion after each injection of current. (C) The stable-state $[Ca^{2+}]$ increases differently in different local Ca^{2+}-IP_3 compartments. The number of compartments with higher $[Ca^{2+}]$ increases after every input. The greater the influx of spike-induced Ca^{2+} entry in a compartment, the sooner the transition in the compartment to the high $[Ca^{2+}]$ state. (D and E) The $[Ca^{2+}]$ and $[IP_3]$ averaged over all the compartments show discrete increases. Note that the concentrations exhibit small-amplitude oscillations in the stable states, implying that the stationary states are not static. (F) A hyperpolarizing input completely inhibits spike firing and lowers the post-stimulus stable firing rate. (G) Stable firing rate decreases with each step current injection. (H) The stable-state $[Ca^{2+}]$ decreases differently in the individual Ca^{2+}-IP_3 compartments. The number of compartments in the high $[Ca^{2+}]$ state is reduced gradually by consecutive inputs. (I and J) The $[Ca^{2+}]$ and $[IP_3]$ averaged over the compartments show discrete decreases.

but not necessarily in the remaining ones (Fig. 5(C)). The greater the peak amplitude of Ca^{2+} influx in a compartment, the earlier a transition to the high $[Ca^{2+}]$ state in that compartment. As the number of activated compartments gradually increased with consecutive inputs, the average $[Ca^{2+}]$ and $[IP_3]$, as well as firing rate, also increased (Fig. 5(D) and (E)).

A strong hyperpolarizing input could completely inhibit persistent firing in the model (Fig. 5(F)). After stimulus presentation, however, the firing rate gradually increased to a stable firing frequency, lower than the pre-stimulus firing rate. Application of consecutive, prolonged hyperpolarizing inputs reduced the persistent firing rate in a graded manner (Fig. 5(G)). In accordance with the rate changes, the stationary $[Ca^{2+}]$ and $[IP_3]$ gradually decreased with consecutive hyperpolarizing inputs (Fig. 5(H)–(J)). As was the case in the single neuron recording experiments, lowering the stable firing rate in our model required a hyperpolarizing input of duration equal to or greater than that of the depolarizing input to induce persistent firing. The maximum conductance of the Ca^{2+}-dependent cation current and the range of j_{Ca} (Fig. 5(H)) were adjusted so that graded rate changes in the model neuron could range from 2–3 Hz to 12–13 Hz, as in the EC cells.

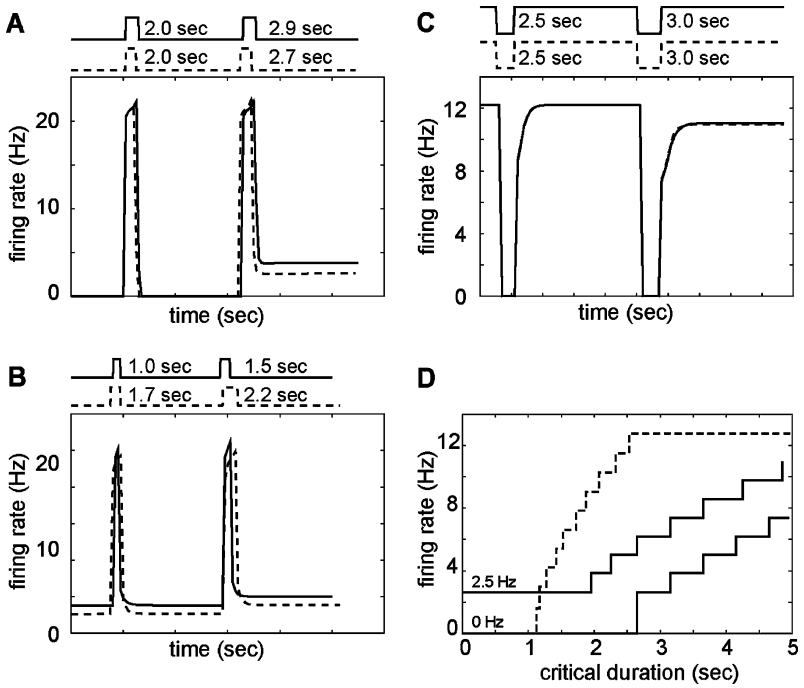

Figure 6. Threshold behaviors exhibited by the model neuron. In (A–C), solid curves represent the responses of the model without Ca^{2+} and IP_3 diffusion effects, whereas dashed curves represent the responses in the presence of the diffusion effects (the neighboring compartments were separated by 25 μm). The corresponding inputs are shown at the top of each panel in a similar manner. (A) A shorter-duration depolarizing current failed to elicit persistent activity, whereas a longer-duration stimulus could induce persistent firing. (B) Similarly, a shorter-duration depolarizing input failed to induce a stable, elevated firing rate in the model neuron initially firing at a low frequency, whereas a longer-duration depolarizing input could elevate the persistent rate. (C) A shorter-duration hyperpolarizing input failed to affect a stable firing rate, whereas a longer-duration input could lower the stable rate. The solid and the dashed curves almost completely overlap each other. (D) The post-stimulus stable firing frequency reached by a depolarizing step current of specified duration is plotted for initial firing rates of 0 Hz and about 2.5 Hz (solid curves). In either case, an input of duration longer than a critical length is required to induce graded rate changes. The dashed curve shows a similar relationship when K_{PLC} is lowered to 0.5 μM in the model.

Stability of the Persistent Activity

Simulations were conducted to show the robustness of the present persistent activity against noise. In these simulations, we included the diffusion of Ca^{2+} and IP_3 between neighboring compartments, assuming that they are separated by 25 μm (see Fig. 9 for details), to confirm that the diffusion effect does not spoil the stability. A sufficiently prolonged depolarizing input triggered persistent firing, whereas a shorter duration input failed to initiate it, in both absence (Fig. 6(A), solid curves) and presence (dashed curve) of the diffusion effect. Similarly, the frequency of persistent firing could be raised or lowered only by a prolonged depolarizing or hyperpolarizing input, respectively, but not by shorter duration inputs (Fig. 6(B) and (C)). In Fig. 6D, we calculated the dependence of graded rate changes on stimulus duration for two different initial neuronal states, i.e., the resting state and a stable firing state (solid curves). Under both conditions, there always exists a critical stimulus duration that is capable of generating a transition to another stable state.

The stability behavior of our model can be understood from the structure of stable states. For any persistent rate change in this model, at least one compartment must be raised to the high $[Ca^{2+}]$ state, and it always takes a finite time for this change to occur (Fig. 4(A)). Therefore, any change to a different attractor state, even to a neighboring attractor state, requires a finite time to cross the boundary between the attractor basins. It is noted that the critical input duration would not vanish even for a greater number of compartments (e.g., $N = 100$: results not shown). The stability behavior of our model is quite analogous to that exhibited by EC cells, providing further experimental support for the proposed mechanism.

Protocol to Change the Critical Input Duration

The necessity of an unnaturally long input questions whether persistent activity of EC cells may underlie working memory, in which transient stimuli typically occur in hundreds of milliseconds. In this model, the prolonged input reflects the fact that the graded rate changes occur near the monostable-bi-stable bifurcation points in parameter space: Near such a bifurcation point, any dynamical system evolves quite slowly compared with the time constant of the system. Below, we argue how the critical input duration can be regulated in the present model.

Figure 7 demonstrates the situation in this model. During the elevation of persistent firing rate, some compartment makes a transition to the high $[Ca^{2+}]$ state. Suppose that during this transition the two curves defined in Fig. 2(B) meet at a single point in the low $[Ca^{2+}]$ region (Fig. 7(A), left panel). Since this point is not stable, the system would move toward a stable fixed point in high $[Ca^{2+}]$ region. In this case, however, the transition takes an infinitely long time, as $d[Ca^{2+}]/dt = 0$ at the low-$[Ca^{2+}]$ fixed point (Fig. 7(A), right panel). This extreme case shows that the transition spends most of the time in leaving the vicinity of the low $[Ca^{2+}]$ state. Therefore, the transition time becomes shorter, if the two curves are separated far apart. As demonstrated by the dashed curves in the figure, reducing K_{PLC} provides a possible way to achieve this. The state change during a hyperpolarizing input can also be understood in a similar fashion (Fig. 7(B)). In this case, the transition to the low $[Ca^{2+}]$ state takes time in leaving the vicinity of the high $[Ca^{2+}]$ state. The transition time can be shortened if two curves are separated sufficiently apart (dashed and gray) by increasing K_{PLC}.

As explained above, reducing K_{PLC} to 0.5 μM significantly shortened the input duration necessary for evoking persistent activity of various firing rates from an initial resting state (Fig. 6(D), dashed curve). The minimum input duration for inducing persistent activity is a rapidly increasing function of K_{PLC} (Fig. 7(C), solid curve). It is remarked that the duration can be as short as about 50 ms at $K_{PLC} = 0.25$ μM (Fig. 7(D)). By contrast, the critical duration of hyperpolarizing input for lowering the stable firing rate is a decreasing function of K_{PLC} (Fig. 7(C), dashed curve). Thus, the same change in K_{PLC} gives opposite effects in increasing and decreasing firing rate.

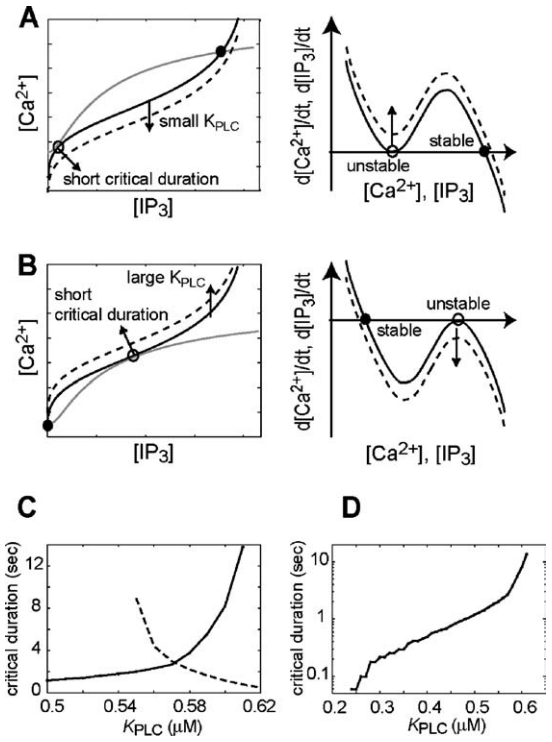

Figure 7. The minimum input duration required for inducing persistent firing in the model. (A) A transition to the high $[Ca^{2+}]$ state takes an infinitely long time at a bifurcation point of the Ca^{2+}-IP_3 dynamics (left panel, gray and solid curves), i.e., in the case that the two curves defined in Fig. 2(B) meet at a single point in the low $[Ca^{2+}]$ region (empty circle). This is because $d[Ca^{2+}]/dt = 0$ at the low-$[Ca^{2+}]$ fixed point (right panel, empty circle). The transition time becomes shorter if the two curves are separated far apart by reducing K_{PLC} (dashed curves). (B) During a hyperpolarizing input, the stationary $[Ca^{2+}]$ must be lowered in some compartment. The transition takes an infinitely long time at a bifurcation point of the Ca^{2+}-IP_3 dynamics (left panel, gray and solid curves). The transition time can be shortened if the two curves are separated sufficiently apart by increasing K_{PLC} (dashed curves). (C) The critical duration of depolarizing input is an increasing function of K_{PLC} (solid curve). On the contrary, the critical duration of hyperpolarizing input becomes a decreasing function. In the latter case, the duration was measured in a model neuron initially firing at 12 Hz. (D) The critical duration of depolarizing input is shown for relatively small values of K_{PLC}. Note that the ordinate is defined in the logarithmic scale.

Crucial Roles of Ca^{2+} and IP_3 in Graded Persistent Firing

The graded persistent activity of our model depends crucially on Ca^{2+} and IP_3 at several steps of the intracellular signaling cascade. In pharmacological experiments, the blockade of L-type Ca^{2+} channels disables persistent firing of EC cells (Egorov et al., 2002). In

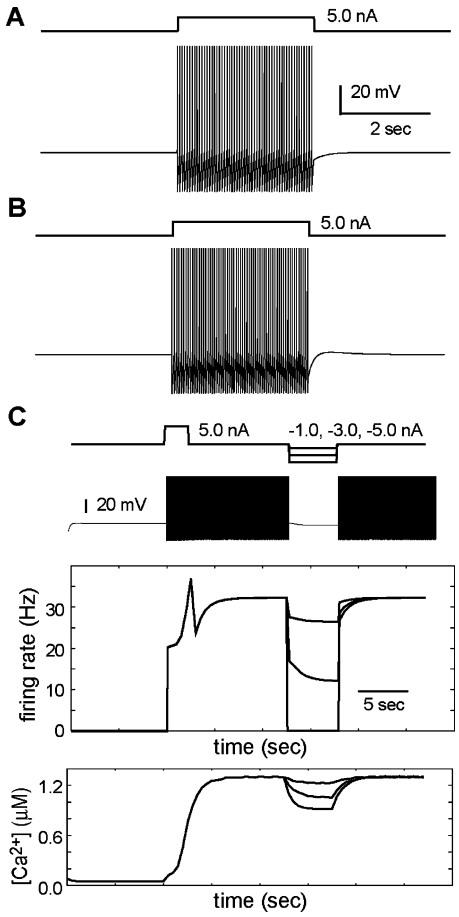

Figure 8. Crucial roles of Ca^{2+}-sensitive PLC activity and inactivation of the IP_3R-channel. (A) If the spike-induced Ca^{2+} entry was blocked, a depolarizing input elicited no persistent firing from the model. (B) A depolarizing step current capable of evoking persistent firing in the normal model failed to do so in the model that lacks Ca^{2+}-sensitive PLC activity ($\alpha = 0$). The only stable state in the truncated model is the resting state. If the baseline $[IP_3]$ is set to a larger value, the truncated model may fire at a unique, constant firing rate (data not shown). In both cases, the graded persistent firing behavior disappears. (C) Inactivation of the IP_3R-channel at high $[Ca^{2+}]$ was partially suppressed by replacing the inactivating variable h with $h^{0.5}$. A depolarizing input evoked a high-frequency firing state (top), in which any hyperpolarizing input was incapable of abating this firing behavior or resetting the neuron in the resting state (middle). The average $[Ca^{2+}]$ shows essentially mono-stable behavior (bottom).

accordance with this, spike-induced Ca^{2+} influx is necessary for triggering calcium release in the model. In Fig. 8(A), the peak intensity of the Ca^{2+} influx was set equal to zero in all the Ca^{2+}-IP_3 compartments. Under this condition, we were unable to induce persistent firing in the model neuron.

In the present model, the bistability of the individual Ca^{2+}-IP_3 compartments emerges from the nonlinear dependence of IP_3 production on $[Ca^{2+}]$ (see the dashed curve in Fig. 2(B)). Therefore, Ca^{2+}-dependent PLC activity is essential for generating the dynamically stable high $[Ca^{2+}]$ states in the model. Figure 8(B) displays the response of the model to a depolarizing step current in the blockade of the Ca^{2+}-dependent PLC activity (i.e., $\alpha = 0$). In this case, $[IP_3]$ was not elevated by spike firing and the IP_3R-channels remained closed during the stimulus. Hence, the evoked activity could not be sustained after the stimulus was terminated.

It seems intriguing to study how a partial blockade of Ca^{2+}-dependent inactivation of the IP_3R-channel influences the multi-stable property of the model. To this end, we re-parameterized the inactivation variable of the IP_3R-channel as $h \to h^{\gamma}$ and set the value of γg at 1/2. This manipulation suppressed the IP_3R-channel closing at high $[Ca^{2+}]$. The case $\gamma = 0$ represents a complete blockade of channel inactivation. In Fig. 8(C) (top and middle), a hyperpolarizing input of various intensity completely inhibited the high-frequency firing evoked by a preceding depolarizing input, but the firing frequency returned to the previous level after the termination of the hyperpolarizing input. Thus, the model neuron has a unique stable state, if the IP_3R-channel exhibits weak or no inactivation. The behavior can be clearly seen in the time course of the average $[Ca^{2+}]$ before, during, and after the input (Fig. 8(C), bottom). It is noted that the complete suppression of neuronal firing failed to return the stationary $[Ca^{2+}]$ to the initial low level. The result indicates that practically no low $[Ca^{2+}]$ state exists in the blockade of the IP_3R-channel inactivation.

Diffusion of Ca^{2+} and IP_3 between Compartments

In most of our previous analyses, we ignored the diffusion of IP_3 and Ca^{2+} within the membrane. In this approximation, the individual compartments essentially behave as independent bi-stable elements, and the multi-stability of an ensemble of the compartments can be guaranteed relatively easily. The multi-stability, however, may collapse due to diffusion, since it tries to uniform molecular concentrations over the compartments. Therefore, we investigated how the diffusion between neighboring compartments affects the graded persistent activity of the model.

Intracellular Ca^{2+} cannot diffuse very far due to fast Ca^{2+} buffering. The diffusion coefficients of buffered

Ca^{2+} and IP_3 are measured as $D_{Ca} = 13$ and $D_{IP_3} = 280\ \mu m^2/s$, respectively, from which the effective diffusion ranges of Ca^{2+} and IP_3 are estimated at 5 and 24 μm (Allbritton et al., 1992). Since the model neuron consists of discrete compartments, the effective diffusion strength depends on the typical length scale, or size L, of a compartment. The parameter L is regarded as the typical distance separating two neughoring compartments, and the diffusion is more influential at smaller L. Below, we show how the multi-stable states degenerate as $1/L$ is increased.

In Fig. 9(A), firing rate of each stable state was calculated for various values of L. As the value of L is decreased, the multi-stable states collapse into bi-stable ones. They can be, however, maintained at L greater than $\sim$25 μm ($1/L < 0.04$). The results are consistent with the estimation of the effective duffusion ranges

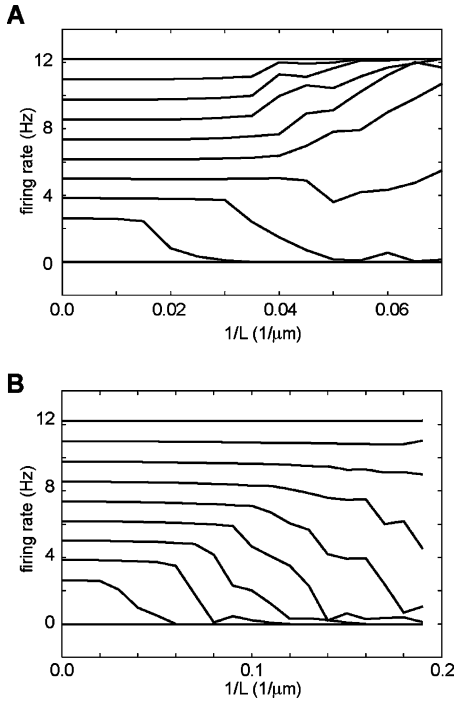

Figure 9. Graded persistent firing influenced by the diffusion of Ca^{2+} and IP_3. To study whether the diffusion of these molecules significantly affects the multi-stable states, all the stable firing rates were calculated assuming physiologically reasonable values of the diffusion constants. The abscissas represent an inverse of the dimension of each Ca^{2+}-IP_3 domain, which can be regarded as the minimum distance to be kept between neighboring compartments. (A) Both Ca^{2+} and IP_3 can diffuse into neighboring compartments. The multi-stable property remains undisturbed as far as each compartment is larger than $\sim$25 μm. (B) Only Ca^{2+} can diffuse. The size of each compartment can be as small as 10–20 μm.

of Ca^{2+} and IP_3. Moreover, the results are consistent with experimental observations that synchronized oscillations of IP_3 and Ca^{2+} are confined in subcellular domains of a length scale smaller than this length (Hirose et al., 1999). We note that the primary cause of the collapse is the diffusion of IP_3 rather than of Ca^{2+}, which can be understood from similar results obtained when only Ca^{2+}, but not IP_3, is diffusive (Fig. 9(B)).

Since the minimum separation required between the compartments is 20–30 μm, a spatial region with a dimension of 200–300 μm can accomodate all 10 compartments. Hence, in pyramidal cells the compartments may be distributed within the soma and the primary shaft of the appical dendrites. Since action potetial backpropagation may fail at the distal dendrites (Spruston et al., 1995), such a compact distribution of the compartmets seems necessary for maintaining the present cellular mechanism robust against the failure in spike-triggered Ca^{2+} entry.

Refilling the Calcium Store Through 'Store-Operated' Channel

So far, we have assumed that $[Ca^{2+}]_{ER}$ is static and is not exhausted by Ca^{2+} release. This assumption was crucial for the bistability of the Ca^{2+}-IP_3 compartments. In fact, the bistability is lost if $[Ca^{2+}]_{ER}$ is treated as a dynamical variable and a balance is enforced in Eq. (1) on the Ca^{2+} fluxes through the ER membrane. In this case, the steady-state cytoplasmic $[Ca^{2+}]$ is determined independent of $[IP_3]$ solely by the balance between the Ca^{2+} influx and efflux through the cell membrane. Then, the nonlinear dependence of the steady $[Ca^{2+}]$ on $[IP_3]$ disappears in Fig. 2, leading to the loss of bistability.

The bistability, however, can be recovered for dynamically changing $[Ca^{2+}]_{ER}$, if the refilling of Ca^{2+} store is included in our model. Accumulating evidence shows that the ER has a specialized calcium refilling mechanism, in which SOCs play a central role. These channels are located on the cell membrane and open when the ER is unloaded, permitting extracellular Ca^{2+} to enter into the sub-SOC-space. The Ca^{2+} in the sub-SOC-space is rapidly pumped into the adjacent ER. The inclusion of SOCs relaxes the condition on the balance of local Ca^{2+} fluxes through the ER membrane (Fig. 10(A)).

Figure 10(B) shows the dependence of the steady $[Ca^{2+}]$ on $[IP_3]$ in the case that both $[Ca^{2+}]$ and $[Ca^{2+}]_{ER}$ are dynamical variables (see Eqs. (10)–(12)).

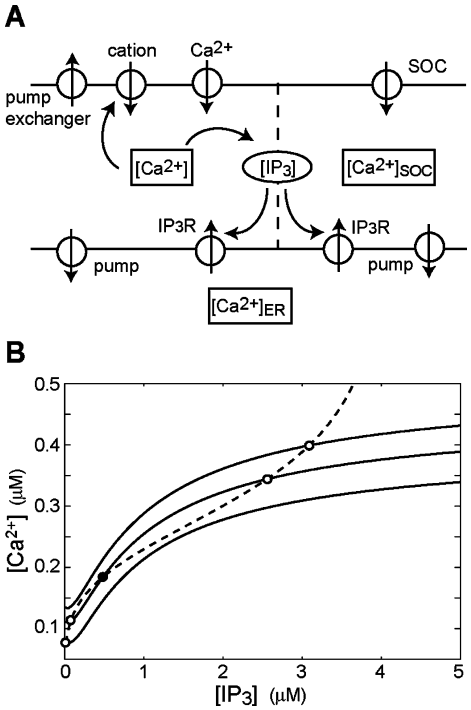

Figure 10. The bi-stable property of $[Ca^{2+}]$-$[IP_3]$ compartments with dynamically variable $[Ca^{2+}]_{ER}$. (A) If $[Ca^{2+}]_{ER}$ is not regarded as constant and ER has no refilling mechanism, each $[Ca^{2+}]$-$[IP_3]$ compartment cannot be bistable. In real neurons, however, Ca^{2+} stores are rapidly refilled by "store-operated" channel (SOC). The refilling process was incorporated into the individual compartments. (B) The rapid refilling of Ca^{2+} stores by SOC can maintain $[Ca^{2+}]_{ER}$ at a sufficiently high steady value during persistent firing. Thus, the bi-stability can be obtained in the individual compartments, as in Fig. 2(B).

Like the previous model, the new model has two stable states in the $[Ca^{2+}]$-$[IP_3]$ phase space. Thus, although the details of the reffiling pathway through SOC must be further clarified by experiments, the refilling process may be crucial for the bistability of the $[Ca^{2+}]$-$[IP_3]$ subcellular compartments.

Discussion

Proposed Roles of IICR and the Implications in Working Memory

Regenerative Ca^{2+} release from the stores is crucial for a variety of cellular activities (Amundson and Clapham, 1993; Thomas et al., 1996; Dolmetsch et al., 1998; Li et al., 1998; Takei et al., 1998; De Koninck and Schulman, 1998; Hirose et al., 1999). In particular, IICR is involved in synapse formation (Sala et al., 2001) and plasticity (Inoue et al., 1998; Nishiyama et al., 2000; Rose and Konnerth, 2001), biological processes which constitute the elementary processes of learning and memory. In this study, we have explicitly modeled a novel role of Ca^{2+} release in mnemonic activity and in computations by single cells. In this model, the bi-stable memory effect produced in local cytoplasmic Ca^{2+} and IP_3 domains plays an essential role in integrating and storing information in persistent output activity. The proposed mechanism can account for the experimental finding on graded persistent activity of EC layer V neurons (Egorov et al., 2002).

Neuronal Ca^{2+} signaling that depends on a binary membrane system has prompted the concept of a "neuron-within-a-neuron" (Berridge, 1998). The outer plasma membrane integrates external information and transmits it by fast-propagating action potentials. Within the neuron, the ER system monitors metabotropic messengers and produces slow regenerative Ca^{2+} signals. The two membrane systems are tied together by a variety of reciprocal interactions to regulate specific neuronal processes. In the proposed single-cell memory, tight bidirectional communications are established by a signaling cascade including spike-induced Ca^{2+} entry through voltage-gated Ca^{2+} channels and Ca^{2+}-activated cation channels on the plasma membrane, PLC activity for IP_3 production, and Ca^{2+} release from IP_3R-channels on the ER.

We have clarified why changing the stable firing rate requires a prolonged stimulus to the model neuron, as in EC cells, by analyzing the bifurcations appearing in the nonlinear dynamics of Ca^{2+} and IP_3. In addition, we have shown that modulating K_{PLC} can easily make the critical input duration as short as some hundred of milliseconds. Although how these modulations can be performed in the brain is unclear, the short input duration is consistent with the typical duration of transient stimuli in working memory. Thus, the present study supports the hypothesis that the graded persistent activity found in single EC cells underlies working memory operation.

Muscarinic modulations are crucial for the graded persistent activity of EC cells, and we can suggest several targets of such modulations in our model. The Ca^{2+}-dependent PLC activity requires activation of muscarinic receptors and a subsequent release of G-protein (Furuichi and Mikoshiba, 1995; Berridge, 1998). Activation of muscarinic receptors is known to enhance different types of Ca^{2+}-activated nonspecific cation current in pyramidal cells (Caeser et al., 1993; Klink and Alonso, 1997; Haj-Dahmane and Andrade,

1999; Fisahn et al., 2002). These facts also add some realities to our model.

Stable States of the Model Neuron

In principle, N bi-stable elements can represent 2^N different stable states, which can be quite large even for relatively small N. In the present model, however, at most N different active states are accessible by consecutive applications of external inputs, because the individual elements can be activated or deactivated only in a fixed order according to their bi-stable firing frequency ranges (Fig. 4).

Generating any rate change between the stable states of the present model requires an external input longer or stronger than a critical one (Fig. 6). The threshold appears not because only a small number of bi-stable elements constitute the present model, but because $[Ca^{2+}]$ must be changed between two discrete levels at least in some element (Fig. 4(A)). If more bi-stable elements are involved, more stable states can be realized and the neighboring states have smaller differences in firing rate (Fig. 6(D)). Nevertheless, the strength of threshold would be unchanged, since it is determined essentially by the property of the single compartments. However, the effective number of bi-stable elements cannot be too large in real neurons, since the diffusion of IP_3 sets the minimum size of independent compartments to $\sim$25 μm (Fig. 9(A)). If the local compartments exist within the soma and the primary shaft of the apical dendrites (350–400-μm long), the effective number will be at most 10–15 for pyramidal cells. It seems intriguing to investigate the number of stable states in EC cells and compare the results with those shown here.

Relationship to Previous Work

Several models have attempted to account for graded persistent activity within the architecture of recurrent neural networks (Cannon et al., 1983; Galiana and Outerbridge, 1984; Seung et al., 2000). These network models have significantly advanced our knowledge about graded persistent activity, but they are limited somewhat because the recurrent connections need to be very finely tuned to generate a continuous attractor state. More recent work shows that the tight precision of parameter tuning can be greatly relaxed if a bi-stable firing property is introduced into the constituent neurons (Koulakov et al., 2002). The present single-cell model is also composed of a large number of bi-stable elements, so it basically requires only moderate tuning of parameters, despite the differences between the network- and single cell-based mechanisms of graded persistent activity. Goldman et al. (2003) also argued the possible role of bistable dendrites in single-cell persistent activity, although the bistability was not modeled in a biologically realistic manner. Neurons in layer II of the EC have been modeled using ionic currents similar to those used in the present model (Fransen et al., 2002). Single EC layer II neurons, however, do not exhibit stable persistent activity, unlike the EC layer V cells (Egorov et al., 2002). The graded persistent activity of EC layer V neurons was recently modeled based on a store-independent mechanism (Fransen et al., 2003).

Very recently, Loewenstein and Sompolinsky proposed a single-cell model to account for graded persistent activity of the goldfish oculomotor neurons (Loewenstein and Sompolinsky, 2003). Their model achieved persistent activity by means of the propagation of a Ca^{2+} wavefront along a homogeneous dendrite. To produce a continuous attractor state, the front was assumed to be stationary at an arbitrary location in the absence of input. The location of the wavefront (i.e., the average $[Ca^{2+}]$) is translated continuously into a stable firing rate by a Ca^{2+}-dependent cation current. The desired property was ensured by tuning the bi-stable property of nonlinear Ca^{2+} dynamics, which might represent the combined effects of Ca^{2+} uptake by pumps and Ca^{2+} release from the stores. The bistability, however, remained to be proved by an explicit modeling of these processes (Wang and Major, 2003).

A crucial difference between our model and the Loewenstein-Sompolinsky model is the role of Ca^{2+} diffusion. The persistent activity of our model is based on the multiple discrete attractor states generated by an ensemble of bi-stable elements. These multiple attractor states collapse in the presence of long-range diffusion effects (Fig. 9). By contrast, in the latter model the diffusion of Ca^{2+} plays an active role in creating a continuous attractor state by Ca^{2+} wavefront. However, the physiological mechanism to have the continuous attractor in real neurons was not fully described and remains to be further clarified.

Experimental Predictions

According to the present proposal, Ca^{2+} release from stores underlies graded persistent activity of cortical

neurons. Simultaneous measurements of [IP_3] and [Ca^{2+}] (Hirose et al., 1999) during persistent firing of layer V EC neurons will allow us to study this mechanism in a straighforward fashion. The mechanism can also be examined by studying whether blocking the IP_3Rs in these cells eliminates persistent firing. On the other hand, blocking the inactivation of IP_3R-channel openings most likely leads to persistent firing at an increased firing frequency and loss of the multiple stable firing states (Fig. 8(C)). It was recently shown that calmodulin plays a crucial role in IP_3R-channel inactivation (Michikawa et al., 1999). Therefore, application of a calmodulin inhibitor to an EC neuron may be an interesting test of the IICR-based mechanism. In addition, we have shown that calcium-dependent IP_3 production is crucial for the mechanism. It is of particular importance to study whether modulating Ca^{2+}-dependent PLC activity may lead to significant changes in the critical input duration, as demonstrated in this study. A complete blockade of the calcium-dependent IP_3 production will eliminate the multi-stable property. In this case, neurons will stay either in the resting state (the case shown in Fig. 8(B)) or in a high-frequency sustained firing state (results not shown) in the absence of external input, depending on the baseline [IP_3] within the membrane. Thus, such a pharmacological manipulation provides another possible test of the proposal that cortical single-cell memory is based on intrinsic Ca^{2+} dynamics involving Ca^{2+} release from the stores.

Acknowledgment

The authors are grateful to K. Mikoshiba and T. Michikawa for discussions on roles of the IP_3Rs in neuronal Ca^{2+} signaling. The authors thank Y. Kang for lectures on Ca^{2+}-activated cation currents and theta-frequency activity of prefrontal neurons. J. T. was supported by the 21st Century COE Program of Japanese Ministry of Education, Culture, Sports, Science and Technology. This work was partially supported by Japan Science and Technology Agencyy.

References

Aksay E, Baker R, Seung HS, Tank DW (2000) Anatomy and discharge properties of pre-motor neurons in the goldfish medulla that have eye-position signals during fixations. J. Neurophysiol. 84: 1035–1049.

Aksay E, Gamkrelidze G, Seung HS, Baker R, Tank DW (2001) In vivo intracellular recording and perturbation of persistent activity in a neural integrator. Nature Neuroscience 4: 184–193.

Allbritton NL, Meyer T, Stryer L (1992) Range of messenger action of calcium ion and inositol 1,4,5-trisphosphate. Science 258: 1812–1815.

Amundson J, Clapham D (1993) Calcium waves. Curr Opin Neurobiol 3: 375–382.

Aoyagi T, Kang Y, Terada N, Kaneko T, Fukai T (2002) The role of Ca^{2+}-dependent cationic current in generating gamma frequency rhythmic bursts: Modeling study. Neuroscience 115: 1127–1138.

Baumann O, Walz B, Somlyo AV, Somlyo AP (1991) Electron probe microanalysis of calcium release and magnesium uptake by endoplasmic reticulum in bee photoreceptors. Proc. Natl. Acad. Sci. USA 88: 741–744.

Berridge MJ (1993) Inositol trisphosphate and calcium signalling. Nature 361: 315–325.

Berridge MJ (1998) Neuronal calcium signaling. Neuron 21: 13–26.

Berridge MJ, Irvine RF (1989) Inositol phosphates and cell signalling. Nature 341: 197–205.

Bezprozvanny I, Watras J, Ehrlich BE (1991) Bell-shaped calcium-response curves of Ins(1,4,5)P_3- and calcium-gated channels from endoplasmic reticulum of cerebellum. Nature 351: 751–754.

Blaustein MP, Golovina VA (2001) Structural complexity and functional diversity of endoplasmic reticulum Ca^{2+} store. Trends in Neuroscience 24: 602–608.

Caeser M, Brown DA, Gähwiler BH, Knöpfel T (1993) Characterization of a calcium-dependent current generating a slow after-depolarization of CA3 pyramidal cells in rat hippocampal slice cultures. Eur. J. Neurosci. 5: 560–569.

Cannon SC, Robinson DA, Shamma S (1983) A proposed neural network for the integrator of the oculomotor system. Biol Cybern 49: 127–136.

De Koninck P, Schulman H (1998) Sensitivity of CaM kinase II to the frequency of Ca^{2+} oscillations. Science 279: 227–230.

De Young GW, Keizer J (1992) A single-pool inositol 1,4,5-trisphosphate-receptor-based model for agonist-stimulated oscillations in Ca^{2+} concentration. Proc. Natl. Acad. Sci. USA 89: 9895–9899.

Delmas P, Crest M, Brown DA (2004) Functional organization of PLC signaling microdomains in neurons. Trends Neurosci. 27: 41–47.

Dolmetsch RE, Xu K, Lewis RS (1998) Calcium oscillations increase the efficiency and specificity of gene expression. Nature 392: 933–936.

Durstewitz D, Seamans JK, Sejnowski TJ (2000) Neurocomputational models of working memory. Nature Neuroscience 3 (Suppl): 1184–1191.

Egorov AV, Hamam BN, Fransen E, Hasselmo ME, Alonso AA (2002) Graded persistent activity in entorhinal cortex neurons. Nature 420: 173–178.

Fiala JC, Grossberg S, Bullock D (1996) Metabotropic glutamate receptor activation in cerebellar Purkinje cells as substrate for adaptive timing of the classically conditioned eye-blink response. J. Neurosci. 16: 3760–3774.

Fisahn A, Yamada M, Duttaroy A, Gan JW, Deng CX, McBain CJ, Wess J (2002) Muscarinic induction of hippocampal gamma oscillations requires coupling of the M1 receptor to two mixed cation currents. Neuron 33: 615–624.

Fransen E, Alonso AA, Hasselmo ME (2002) Simulations of the role of the muscarinic-activated calcium-sensitive nonspecific cation current INCM in entorhinal neuronal activity during delayed matching tasks. J. Neurosci. 22: 1081–1097.

Fransen E, Egorov AV, Hasselmo ME, Alonso AA (2003) Model of graded persistent activity in entorhinal cortex neurons. Abs Soc Neurosci: Program # 557.6.

Furuichi T, Mikoshiba K (1995) Inositol 1, 4, 5-trisphosphate receptor-mediated Ca^{2+} signaling in the brain. J. Neurochem. 64: 953–960.

Galiana HL, Outerbridge JS (1984) A bilateral model for central neural pathways in vestibuloocular reflex. J. Neurophysiol. 51: 210–241.

Goldman MS, Levine JH, Major G, Tank DW, Seung HS (2003) Robust persistent neural activity in a model integrator with multiple hysteretic dendrites per neuron. Cerebral Cortex 13: 1185–1195.

Haj-Dahmane S, Andrade R (1999) Muscarinic receptors regulate two different calcium-dependent non-selective cation currents in rat prefrontal cortex. Eur. J. Neurosci. 11: 1973–1980.

Hernández A, Zainos A, Romo R (2002) Temporal evolution of a decision-making process in medial premotor cortex. Neuron 33: 959–972.

Hirose K, Kadowaki S, Tanabe M, Takeshima H, Iino M (1999) Spatiotemporal dynamics of inositol 1,4,5-trisphosphate that underlies complex Ca^{2+} mobilization patterns. Science 284: 1527–1530.

Inoue T, Kato K, Kohda K, Mikoshiba K (1998) Type 1 inositol 1,4,5-trisphosphate receptor is required for induction of long-term depression in cerebellar Purkinje neurons. J. Neurosci. 18: 5366–5373.

Kang Y, Okada T, Ohmori H (1998) A phenytoin-sensitive cationic current participates in generating the afterdepolarization and burst afterdischarge in rat neocortical pyramidal cells. Eur. J. Neurosci. 10: 1363–1375.

Keller EL, Kamath BY (1975) Characteristics of head rotation and eye movement-related neurons in alert monkey vestibular nucleus. Brain Res. 100: 182–187.

Kitano K, Câteau H, Fukai T (2002) Self-organization of memory activity through spike-timing-dependent plasticity. Neuroreport 13: 795–798.

Klink R, Alonso A (1997) Ionic mechanisms of muscarinic depolarization in entorhinal cortex layer II neurons. J. Neurophysiol. 77: 1829–1843.

Koulakov AA, Raghavachari S, Kepecs A, Lisman JE (2002) Model for a robust neural integrator. Nature Neuroscience 5: 775–782.

Li W, Llopis J, Whitney M, Zlokarnik G, Tsien RY (1998) Cell-permeant caged InsP3 ester shows that Ca^{2+} spike frequency can optimize gene expression. Nature 392: 936–941.

Loewenstein Y, Sompolinsky H (2003) Temporal integration by calcium dynamics in a model neuron. Nature Neuroscience 6: 961–967.

Meyer T, Stryer L (1988) Molecular model for receptor-stimulated calcium spiking. Proc. Natl. Acad. Sci. USA 85: 5051–5055.

Michikawa T, Hirota J, Kawano S, Hiraoka M, Yamada M, Furuichi T, Mikoshiba K (1999) Calmodulin mediates calcium-dependent inactivation of the cerebellar type 1 inositol 1,4,5-trisphosphate receptor. Neuron 23: 799–808.

Mignery GA, Johnston PA, Sudhof TC (1992) Mechanism of Ca^{2+} inhibition of inositol 1,4,5-trisphosphate ($InsP_3$) binding to the cerebellar $InsP_3$ receptor. J. Biol. Chem. 267: 7450–7455.

Nakamura T, Barbara JG, Nakamura K, Ross WN (1999) Synergistic release of Ca^{2+} from IP_3-sensitive stores evoked by synaptic activation of mGluRs paired with backpropagating action potentials. Neuron 24: 727–737.

Nakamura T, Nakamura K, Lasser-Ross N, Barbara JG, Sandler VM, Ross WN (2000) Inositol 1,4,5-trisphosphate (IP_3)-mediated Ca^{2+} release evoked by metabotropic agonists and backpropagating action potentials in hippocampal CA1 pyramidal neurons. J. Neurosci. 20: 8365–8376.

Nishiyama M, Hong K, Mikoshiba K, Poo MM, Kato K (2000) Calcium stores regulate the polarity and input specificity of synaptic modification. Nature 408: 584–588.

Parekh AB, Penner R (1997) Store depletion and calcium influx. Physiol. Rev. 77: 901–930.

Partridge LD, Valenzuela CF (1999) Ca^{2+} store-dependent potentiation of Ca^{2+}-activated non-selective cation channels in rat hippocampal neurones in vitro. J. Physiol. (Lond) 521 (Pt 3): 617–627.

Putney JW Jr, Ribeiro CM (2000) Signaling pathways between the plasma membrane and endoplasmic reticulum calcium stores. Cell. Mol. Life Sci. 57: 1272–1286.

Romo R, Brody CD, Hernandez A, Lemus L (1999) Neuronal correlates of parametric working memory in the prefrontal cortex. Nature 399: 470–473.

Rose CR, Konnerth A (2001) Stores not just for storage. intracellular calcium release and synaptic plasticity. Neuron 31: 519–522.

Rosen MJ (1972) A theoretical neural integrator. IEEE Trans. Biomed. Eng. 19: 362–367.

Sala C, Piëch V, Wilson NR, Passafaro M, Liu G, Sheng M (2001) Regulation of dendritic spine morphology and synaptic function by Shank and Homer. Neuron 31: 115–130.

Seung HS, Lee DD, Reis BY, Tank DW (2000) Stability of the memory of eye position in a recurrent network of conductance-based model neurons. Neuron 26: 259–271.

Shadlen MN, Newsome WT (2001) Neural basis of a perceptual decision in the parietal cortex (area LIP) of the rhesus monkey. J. Neurophysiol. 86: 1916–1936.

Sharp AH, McPherson PS, Dawson TM, Aoki C, Campbell KP, Snyder SH (1993) Differential immunohistochemical localization of inositol 1,4,5-trisphosphate- and ryanodine-sensitive Ca^{2+} release channels in rat brain. J. Neurosci. 13: 3051–3063.

Spruston N, Schiller Y, Stuart G, Sakmann B (1995) Activity-dependent action potential invasion and calcium influx into hippocampal CA1 dendrites. Science 268: 297–300.

Takei K, Shin RM, Inoue T, Kato K, Mikoshiba K (1998) Regulation of nerve growth mediated by inositol 1,4,5-trisphosphate receptors in growth cones. Science 282: 1705–1708.

Thomas AP, Bird GS, Hajnóczky G, Robb-Gaspers LD, Putney JW (1996) Spatial and temporal aspects of cellular calcium signaling. FASEB J. 10: 1505–1517.

Walker JW, Somlyo AV, Goldman YE, Somlyo AP, Trentham DR (1987) Kinetics of smooth and skeletal muscle activation by laser pulse photolysis of caged inositol 1,4,5-trisphosphate. Nature 327: 249–252.

Wang SS, Alousi AA, Thompson SH (1995) The lifetime of inositol 1,4,5-trisphosphate in single cells. J. Gen. Physiol. 105: 149–171.

Wang XJ (1999) Synaptic basis of cortical persistent activity: The importance of NMDA receptors to working memory. J. Neurosci. 19: 9587–9603.

Wang SS, Major G (2003) Integrating over time with dendritic wavefronts. Nature Neuroscience 6: 906–908.

Wagner J, Fall CP, Hong F, Sims CE, Allbritton NL, Fontanilla RA, Moraru II, Loew LM, Nuccitelli R (2004) A wave of IP_3 production accompanies the fertilization Ca^{2+} wave in the egg of the frog, *Xenopus laevis*: Theoretical and experimental support. Cell Calcium 35: 433–447.

Yamada WM, Koch C, Adams PR (1998) Multiple channels and calcium dynamics. In: C Koch, I Segev, eds. Methods in Neuronal Modeling: From Ions to Networks. The MIT Press, Cambridge pp. 137–170.